Anharmonic behavior and structural phase transition in Yb2O3

Sugandha Dogra Pandey, K. Samanta, Jasveer Singh, Nita Dilawar Sharma, and A. K. Bandyopadhyay

Citation: AIP Advances **3**, 122123 (2013); doi: 10.1063/1.4858421
View online: http://dx.doi.org/10.1063/1.4858421
View Table of Contents: http://scitation.aip.org/content/aip/journal/adva/3/12?ver=pdfcov
Published by the AIP Publishing

Anharmonic behavior and structural phase transition in Yb_2O_3

Sugandha Dogra Pandey, K. Samanta, Jasveer Singh,
Nita Dilawar Sharma,[a] and A. K. Bandyopadhyay
Vacuum & Pressure Standards, National Physical Laboratory, New Delhi-110012, India

(Received 30 September 2013; accepted 10 December 2013; published online 31 December 2013)

The investigation of structural phase transition and anharmonic behavior of Yb_2O_3 has been carried out by high-pressure and temperature dependent Raman scattering studies respectively. *In situ* Raman studies under high pressure were carried out in a diamond anvil cell at room temperature which indicate a structural transition from cubic to hexagonal phase at and above 20.6 GPa. In the decompression cycle, Yb_2O_3 retained its high pressure phase. We have observed a Stark line in the Raman spectra at 337.5 cm^{-1} which arises from the electronic transition between $^2F_{5/2}$ and $^2F_{7/2}$ multiplates of Yb^{3+} ($4f^{13}$) levels. These were followed by temperature dependent Raman studies in the range of 80–440 K, which show an unusual mode hardening with increasing temperature. The hardening of the most dominant mode ($T_g + A_g$) was analyzed in light of the theory of anharmonic phonon-phonon interaction and thermal expansion of the lattice. Using the mode Grüneisen parameter obtained from high pressure Raman measurements; we have calculated total anharmonicity of the $T_g + A_g$ mode from the temperature dependent Raman data. [http://dx.doi.org/10.1063/1.4858421]

I. INTRODUCTION

The rare earth (RE) sesquioxides [Re_2O_3] attract an enormous research interest from both technological as well as fundamental point of view.[1] They are excellent host materials for solid state lasers[2] and improved phosphors.[3,4] They have high thermal stability and toughness suitable for their application in refractors or abrasives.[5] At ambient, the RE oxides exist in three polymorphic phases: for large cationic radius (La to Nd), the hexagonal phase designated as the *A*-type with a space group $P\bar{3}m1$ is the most stable; for the medium cations (Sm to Gd), the monoclinic phase designated as *B*-type with space group C_2/m is preferred; and for the small cations (Tb to Lu), the cubic-phase designated as *C*-type with space group $Ia\bar{3}$ is the most stable.[6,7]

The high pressure studies of RE sesquioxides are a subject of fundamental research; particularly to address the problems of stability and structural transformation, metal-insulator transition, enhancement or collapse of magnetic ordering, and amorphization, etc. Under such conditions the bonding patterns established for the systems near ambient conditions change dramatically, causing profound effects on numerous physical and chemical properties and leading to the formation of new classes of materials. The investigations on pressure induced phase transition of *C*-type RE oxides (e.g. Yb_2O_3, Er_2O_3, Sc_2O_3, Ho_2O_3, and Y_2O_3) have been reported by using energy dispersive x-ray diffraction (EDXD).[7–11] There have also been reports on the high pressure behavior of other RE sesquioxides.[12–17]

Among the *C*-type RE sesquioxides, Yb_2O_3 is of particular interest because Ytterbium (*Yb*, f^{13}) is one of the anomalous rare earth elements, whose oxide exhibits anomalous wavenumber decrease in the Raman modes, particularly the $T_g + A_g$ mode. The anomalies correlate with

[a]Corresponding E-mails: ndilawar@mail.nplindia.org (Nita Dilawar Sharma)

the thermodynamic properties and weaker bonding in Yb_2O_3. This weaker bonding is related to unique properties of Yb as a metal, which include minima in melting point and heat of vaporization, as well as relative maxima in atomic radii/volume, and also in compounds with other oxidation states.[18] It is also suggested that these anomalies are caused by the electron-phonon interaction involving low-lying *f*-states which are below the Fermi level for Ytterbium.[18] In the cubic phase the *Yb* atoms occupy two octahedral sites; eight atoms in (*a*) positions with three-fold inversion symmetry C_{3i}, and 24 atoms in (*d*) positions with two-fold symmetry C_2. For the C_{3i} site two oxygen atoms are missing across the body diagonal while for the C_2 site they are missing across a face diagonal.[7]

It is well known that Raman scattering is one of the most powerful techniques to investigate the phonon spectrum, electron phonon coupling, structural phase transitions, and anharmonic behavior of the optical modes. Raman spectroscopic investigations of the high pressure phases of nano-crystalline Eu_2O_3,[19] Y_2O_3, Gd_2O_3, Sm_2O_3,[20] and Dy_2O_3[21] have already been reported. Meyer *et al.* have reported the structural phase transition of *C*-type Yb_2O_3 to the monoclinic *B*-type at 13 GPa in high pressure EDXD measurement and the same was observed at 20 GPa in high pressure Mössbauer measurement at 4.2 K.[7] Hoekstra *et al.*[12] obtained B-type Yb_2O_3 from C-type at 40 kbar and 1000^0C and the transition was found to be irreversible. Recently Yusa *et al.*[22] also demonstrated the conversion of C-type Yb_2O_3 into A-type at 19.6 GPa through an intermediate B-type phase which was observed at 15.9 GPa. Recently Lonappan[23] reported high pressure Raman data on single crystal Yb_2O_3. However, to the best of our knowledge, there are no reports on combined studies on high pressure Raman scattering to investigate the phase transition as well as the anharmonic behavior of optical phonons as a function of temperature. In this article, we are reporting a detailed Raman scattering investigation of Yb_2O_3 as a function of pressure as well as temperature.

II. EXPERIMENTAL

Commercially available Yb_2O_3 powder was used for the present study and no pre-treatment was done. The slow scan XRD of the Yb_2O_3 powder was carried out by Bruker D-8 Advance powder X-Ray diffractometer using Cu k_α ($\lambda = 1.5404$ Å) radiation.

The high-pressure Raman scattering studies were carried out with a single stage Jobin-Yvon Spex monochromator using an Ar^+ ($\lambda = 514.5$ nm) ion laser. The Raman signal was detected by water cooled photomultiplier tube (PMT). A Mao-Bell type diamond anvil cell (DAC) with octagonal flats having about 400 μm diameter culets was used to generate high pressure up to 28 GPa. The sample was loaded in the drilled gasket hole along with a few small ruby chips (5–10 μm) for monitoring the pressure. The pressure transmitting medium used was methanol: ethanol in the ratio of 4:1.

Temperature dependent Raman measurements were performed in the backscattering geometry using the Jobin-Yvon T64000 Triple-mate instrument coupled with the Ar^+ 514.5 nm laser line. A charge-coupled device system with the accuracy of (0.5 cm^{-1}) was used to collect the scattered data. The sample temperature was varied from 80–440 K by using a continuous flow LN_2 optical cryostat in which the sample compartment was maintained at a pressure of $\sim 10^{-6}$ torr using a turbo-molecular pump.

III. RESULTS AND DISCUSSION

Figure 1 shows the x-ray diffraction pattern obtained from the sample under investigation. The diffracting peaks agreed well with the JCPDS data card number 43–1037 for cubic phase of Yb_2O_3. The crystallite size of Yb_2O_3 was estimated as $\sim$96 nm by using Debye-Scherrer relation.

The Raman spectrum of Yb_2O_3 powder obtained under ambient conditions is shown in Figure 2. As mentioned, the cubic Yb_2O_3 belongs to the space group $Ia\bar{3}(T_h^7)$ having 16 formula units per primitive cell. There are 32 *Yb*-ions, 24 in (*d*) sites with C_2 symmetry, and 8 in (*b*) sites with site symmetry C_{3i}. There are 48 oxygen atoms in the body-centered cell having

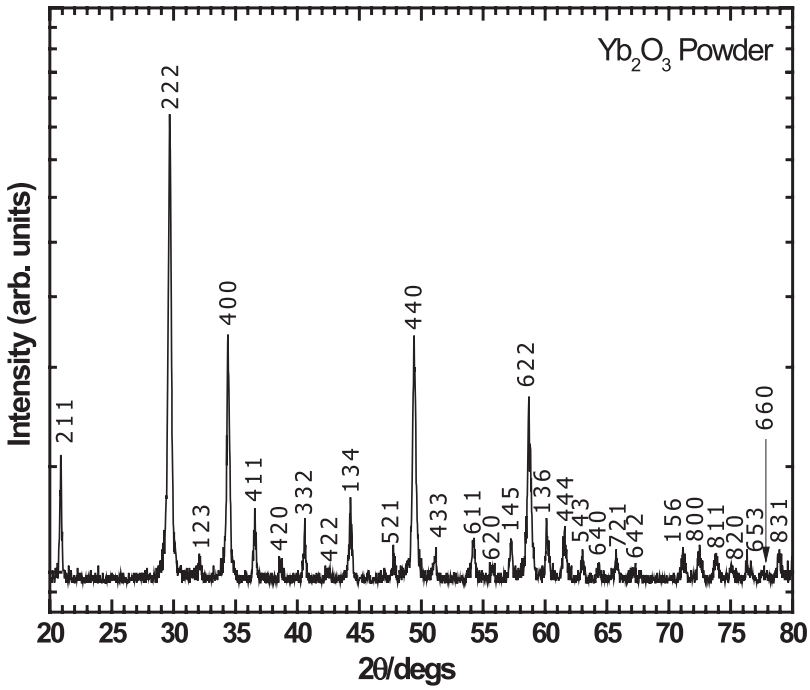

FIG. 1. X-ray diffraction patterns for Yb_2O_3 powders.

site symmetry C_1.[24] The irreducible representations of vibrations of atoms occupying the sites are:

$$C_2\,(Yb) : A_g + A_u + E_g + E_u + 5T_g + 5T_u \tag{1a}$$

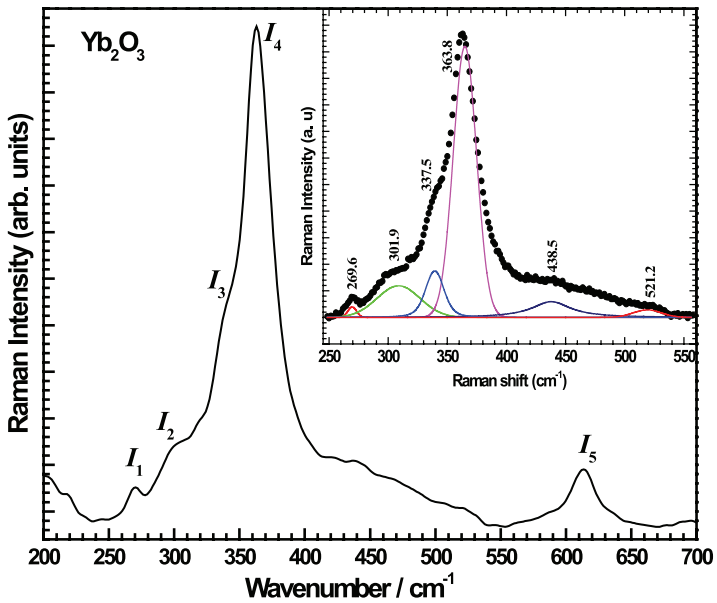

FIG. 2. Raman spectra for Yb_2O_3 powder at ambient; inset shows the fitting of Yb_2O_3 Raman spectra at ambient. The shoulder region is the combination of two peaks.

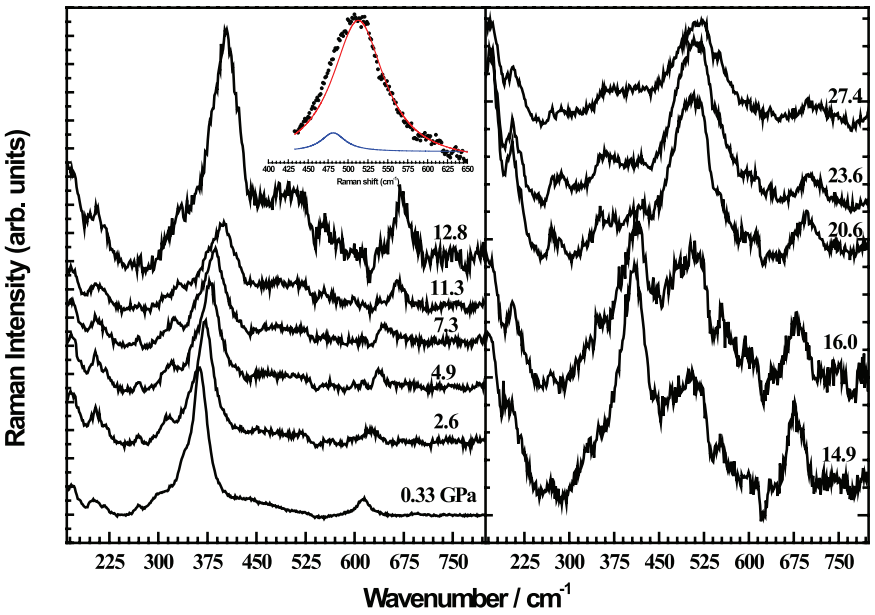

FIG. 3. Pressure dependent Raman spectra of Yb_2O_3 at room temperature; left inset shows the deconvolution of 515 cm^{-1} peak at 27.4 GPa.

$$C_{3i}\,(Yb) : A_u + E_u + T_u \tag{1b}$$

$$C_1\,(O) : 3A_g + 3E_g + 9T_g \tag{1c}$$

The eight rigid *Yb* atoms at C_{3i} site do not contribute to the Raman active optical modes, but give acoustic branch of $A_u + E_u$ and infrared active T_u mode. Hence, the 22 Raman active optical modes of cubic Yb_2O_3 at ambient are:

$$\Gamma = 4A_g + 4E_g + 14T_g \tag{2}$$

However, smaller numbers of modes are observed in the Raman spectra; this may be due to the fact that some of the observed modes are actually superposition of closely spaced different type of modes, which are un-separated owing to a weak factor-group interaction.[6]

As shown in Figure 2, we have observed five distinct lines (I_1–I_5) at 269.6, 301.9, 337.5, 363.8, and 613.5 cm^{-1}, and a wide shoulder in the range of 400–545 cm^{-1}. The lines (I_1–I_5) are assigned as the $T_g + E_g$, E_g, $\Gamma_{el}(C_{3i})$, $T_g + A_g$, and T_g, respectively; the observed line I_3, at 337.5 cm^{-1} is referred to as a Stark level assignment for Yb^{3+} ion in C_{3i} site.[25] In the case of *C*-type Yb_2O_3, the Yb^{3+} ion in C_{3i} sites have electronic configuration $Yb^{3+}(Xe\ 4d^{10}4f^{13}5s^25p^6)$, the spin-orbit and crystal-field interaction splits the *f*-orbital into the multiplets of $^2F_{7/2}$ and $^2F_{5/2}$ levels. The electronic transition from the ground state of $^2F_{7/2}$ to the $^2F_{5/2}$ level gives the Stark line at 337.5 cm^{-1}.[26]

The shoulder region (400–545 cm^{-1}) is effectively the combination of two peaks at 442.3 and 521.2 cm^{-1}. The peak at 442.3 cm^{-1} is corresponding to the T_g mode and other one is unidentified; however this mode persists and its intensity increases gradually with increase of pressure; which will be discussed later.

Pressure dependent Raman measurement of Yb_2O_3 sample taken at room temperature, is shown in Fig. 3. It is observed that the most intense I_4 peak at 363.8 cm^{-1} progressively loses intensity and disappears at and above ~21 GPa, and the emerging peaks at ~510 cm^{-1} dominate. When the pressure increases, new Raman modes emerge at ~483.5 and 517.8 cm^{-1} at and above 11.3 GPa, particularly these two modes consistently increase their intensity and further develop in to well defined peaks. One can see from Fig. 3 that the main peak (363.8 cm^{-1}) of cubic Yb_2O_3 phase coexists with the emerging modes of new phase in a wide pressure region. At the maximum

experimental pressure of 27.4 GPa, the most prominent peak at ~515 cm^{-1} is basically the combination of two peaks at ~484.8 and 512.6 cm^{-1}, as shown in the inset of Fig. 3. This new phase has been identified as the hexagonal phase. It has been reported that for the A-type Ln_2O_3, four Raman active optical modes are present corresponding to the two stretching vibrations, i.e. A_{1g} and E_g, and two bending vibrations of the A_{1g} and E_g.[11,27]

Hence, above the transition pressure, the cubic Yb_2O_3 transforms to hexagonal phase (*A*) which belongs to the space group $P\bar{3}m1(D^3_{3d})$. The two *Yb* atoms and two oxygen atoms are in the (2*d*) position with site symmetry C_{3v}, and the remaining oxygen atom is in the (1*a*) position with site symmetry D_{3d}. The oxygen atom at (1*a*) position is octrahedrally surrounded by six *Yb*-atoms; whereas, the same at (2*d*) position are surrounded by *Yb* atoms at the corner of the slightly distorted tetrahedron.[27] The irreducible representations of the vibrations of the atoms in hexagonal Yb_2O_3 phase are:

$$C_{3v}(Yb) : A_{1g} + A_{2u} + E_g + E_u \tag{3a}$$

$$C_{3v}(O) : A_{1g} + A_{2u} + E_g + E_u \tag{3b}$$

$$D_{3d}(O) : A_{2u} + E_u \tag{3c}$$

Hence, the Raman active optical modes of the hexagonal Yb_2O_3 are:

$$\Gamma = 2A_{1g} + 2E_g \tag{4}$$

Out of these, the bending vibrations occur at low wave-numbers, typically between 100 and 200 cm^{-1}, while the stretching vibrations occur at higher wave-numbers between 400 and 550 cm^{-1}. In analogy with the previously reported modes for the hexagonal phases,[27] the mode at ~484.8 may be identified as the A_{1g} and the mode at 512.6 cm^{-1} may be assigned to the E_g mode. It may be pertinent to point out here that according to Shaack and Koningston,[6] Yb_2O_3 is known to behave differently from all other rare earth sesquioxides where the Raman lines are considerably broadened. This observation is consistent with the present result.

The pressure dependent frequency shifts of Yb_2O_3 are observed in Fig. 4. Most cubic phase peaks are seen shifting to higher frequency with an increase in pressure. The new modes corresponding to the hexagonal phase can be seen at and above 11.3 GPa which interestingly do not show significant shift with increase in applied pressure. The error bars are plotted to account for the non-hydrostatic pressure components.

The pressure coefficients of the observed cubic phase Raman modes (as listed in Table I) are obtained from the linear fitting using the equation:

$$\omega = \omega_0 + (d\omega/dP)\,P \tag{5}$$

We have calculated the mode Grüneisen parameters using the following equation.

$$\gamma_i = (B_0/\omega_0)(d\omega/dP) \tag{6}$$

Where, B_0 is the isothermal bulk modulus (181 GPa) of Yb_2O_3 at cubic phase,[7,28] ω_0 is the mode frequency at ambient.

On decompression, as the pressure is released, the observed peaks shift towards lower frequency side and the intensity decreases as shown in Fig. 5. However, the starting cubic phase is not recovered at total release. Instead the most prominent band at about 513 cm^{-1} at 27.4 GPa splits into a doublet on total release, with peaks centered at 493 and 525 cm^{-1}. This observation further confirms the formation of hexagonal (A) phase at high pressure, which is irreversible on decompression.

The hexagonal phase of rare earth sesquioxides belong to the smallest molar volume as compared to monoclinic and cubic phases; thus the hexagonal phase formation is more favorable under the application of external pressure. The relationship between cubic (*C*) and monoclinic (*B*) structures is not simple because the rare earth atoms are displaced with respect to the oxygen during transition from *C* to *B*. The *C* to *B* transformation is reconstructive while *C* to *A* is displacive. It seems that

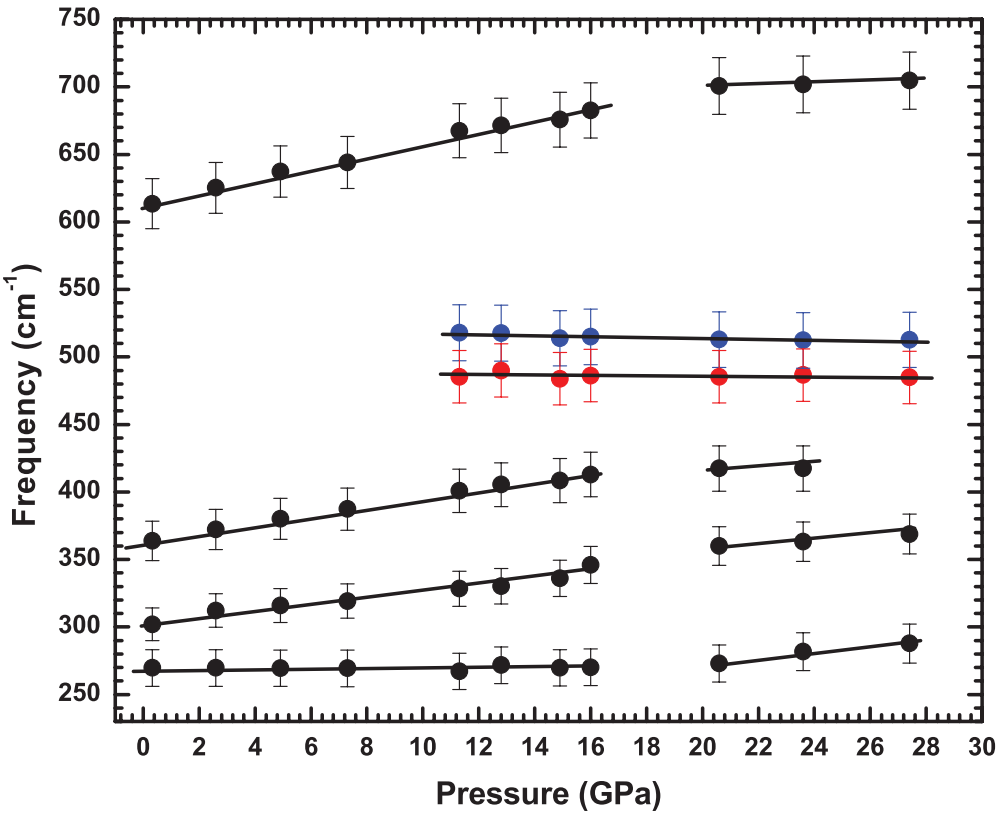

FIG. 4. The observed Raman frequency shift of Yb_2O_3 taken at room temperature, as function of pressure.

TABLE I. The mode frequencies, pressure coefficients, and Grüneisen parameters (γ_i) for phonon modes in cubic Yb_2O_3.

ω (cm^{-1})	$d\omega/dp$ (cm^{-1}/GPa)	γ_i
269.6	0.031	0.02
301.9	2.364	1.417
363.8	3.102	1.543
613.5	4.363	1.287

the slightly different experimental conditions seem to favor either *B* or *A* phase.[7] The *B* to *A* or *A* to *B* transition requires lesser energy as it is displacive type. In this context, it is relevant to mention here that Zhang *et al*.[29] also reported a phase diagram for Gd_2O_3 according to which at low temperatures, the cubic to hexagonal phase transition is favored with application of pressure while at high temperatures, the monoclinic phase is favored. Since the kinetics of phase transformation depend in general on the pressure, temperature and the amount of non-hydrostatic stresses as well as the existence of defects; the barrier heights for transformation would also depend on these parameters.[30]

To investigate the anharmonic behavior of optical phonons, we have studied the temperature dependent Raman spectra of Yb_2O_3 in the range of 80–440 K. The spectrum of Yb_2O_3 at 80 K (Fig. 6) shows modes at 281.3, 306.4, 332.7, 357.8, 419.9, and 435.6 cm^{-1}, corresponding to the $T_g + E_g$, E_g, Γ_{el}, $T_g + A_g$, and two T_g, respectively.[6] It is interesting to observe the electronic contribution (Γ_{el}) at 332.7 cm^{-1}.[25,26] It is also significant to point out that the shoulder region i.e. 400–550 cm^{-1} region which showed very weak peaks at ambient shows well defined peaks at 80 K.

The temperature dependent micro-Raman study of Yb_2O_3 indicates more complex behavior. Observed from the Fig. 7 is the unusual hardening of $T_g + A_g$ mode at 357.8 cm^{-1} upon heating;

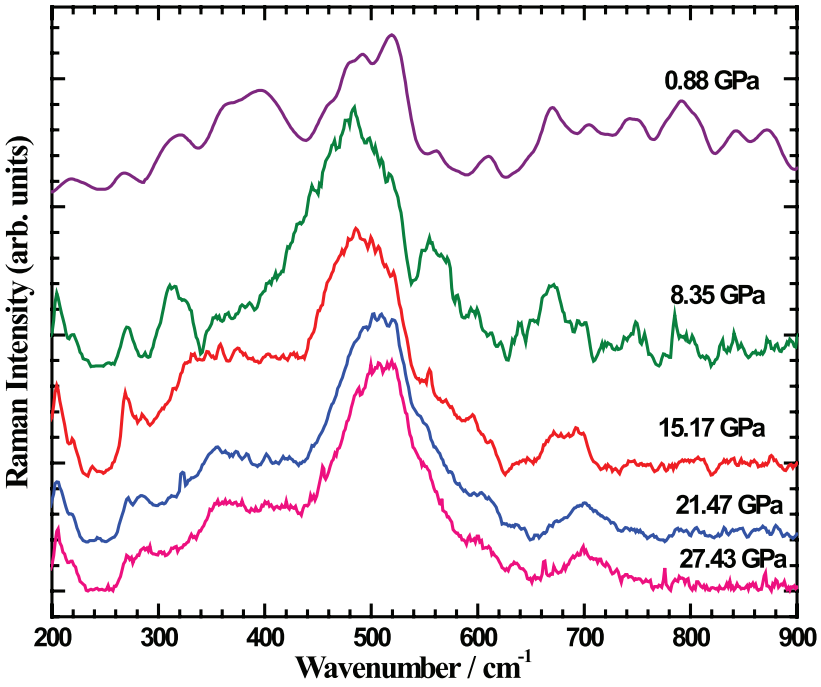

FIG. 5. Decompression cycle for Yb_2O_3 at room temperature; the phase transition is irreversible.

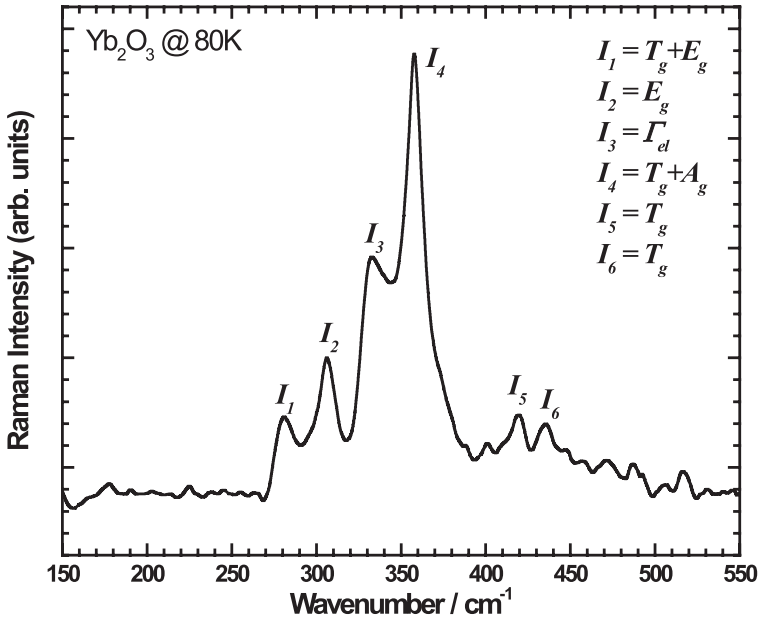

FIG. 6. Raman spectrum of Yb_2O_3 recorded at 80 K.

whereas the modes at 281.3, 306.4, 419.9, and 435.6 cm^{-1} do not show any significant shift within the temperature range 80–440 K; but they gradually lose their intensity, become broadened, and finally disappear above 370 K. The considerable change is observed in the most intense peak $T_g + A_g$ at 357.8 cm^{-1}. The frequency shift for this mode in the temperature range 80–190 K is low; however, there is a significant shift of frequency (~ 7 cm^{-1}) above 200K and up to 440 K. A dashed straight guide line in Fig. 7 gives better recognition of frequency shift. From Fig. 8 too, where the

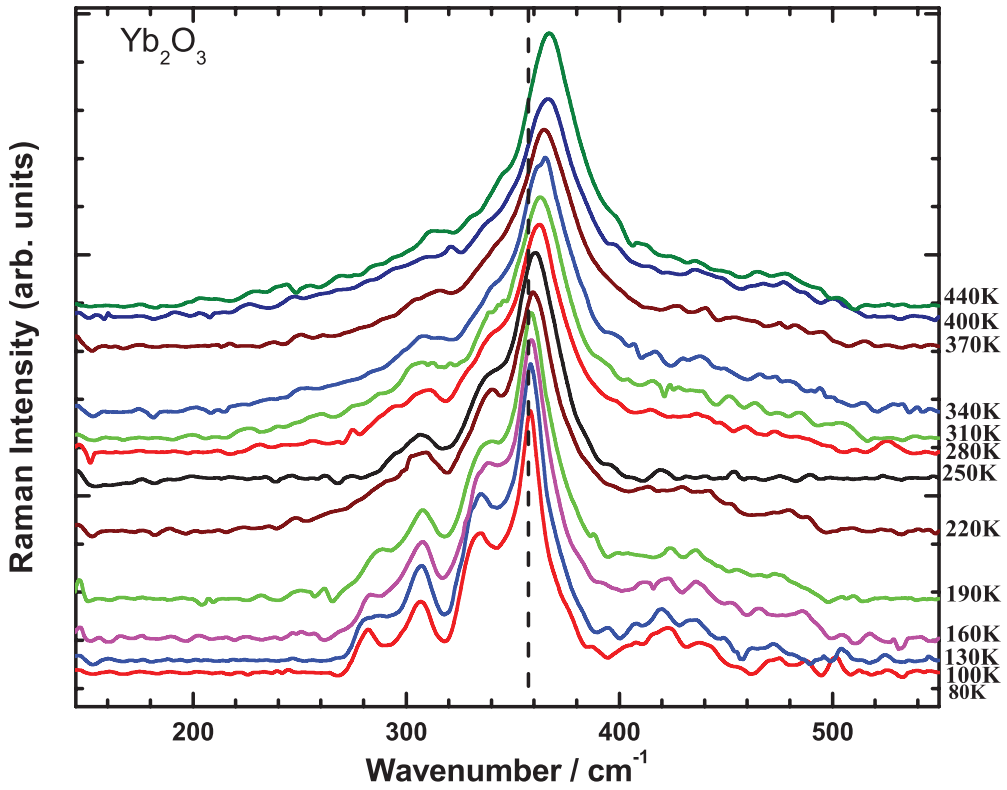

FIG. 7. Temperature dependent phonon behavior of Yb_2O_3 in the range 80–440 K.

experimental points are plotted, one can see the anomalous mode hardening as the peak frequency shifts towards higher frequency side with increasing temperature.

It is known that the variation of the frequency of normal modes with change in temperature at a constant pressure arises from contributions from volume expansion and anharmonicity. The latter in turn arises from cubic and quartic anharmonicities (self-energy shift). The complete expression for the frequency as a function of temperature can be explained as:[31]

$$\omega(T) = \omega_0 + (\Delta\omega)_{latt} + (\Delta\omega)_{anh} \tag{7}$$

Where, ω_0 is the harmonic frequency, which was obtained as 357.8 cm^{-1}, extrapolating the experimental data down to 80 K; the quasi-harmonic term $(\omega)_{latt}$ accounts for the lattice expansion contribution; and $(\omega)_{anh}$ is the intrinsic (true) anharmonic contribution due to cubic and quatric anharmonicities. In the most solids of positively expanding lattice, phonon mode softening results as a function of increase in temperature. The quasi-harmonic contribution can be explained as:[31]

$$(\Delta\omega)_{latt} = \omega_0 \left\{ exp\left[-\gamma_i \int_0^T 3\alpha(T)\, dT \right] - 1 \right\} \tag{8}$$

Where, γ_i (= 1.543) is the mode Grüneisen parameter of the $T_g + A_g$ mode obtained from the pressure dependent data above, and α (= 6.6×10^{-6}/K) is the linear thermal expansion coefficient of Yb_2O_3. The anharmonic contribution $(\omega)_{anh}$ arises from the phonon-phonon interaction due to the lowest-order cubic and quartic terms in the inter-atomic potential. The anharmonic contribution as a function of temperature can be explained as:[32]

$$(\Delta\omega)_{anh} = A\left[1 + \frac{2}{\exp(\hbar\omega_0/2\mathrm{kT}) - 1}\right] + B\left[1 + \frac{3}{\exp(hw_0/3k\mathrm{T}) - 1} + \frac{3}{(\exp(hw_0/3k\mathrm{T}) - 1)^2}\right] \tag{9}$$

The first term describes the coupling of an optical phonon to two low-energy phonons (three phonon process); the second term is due to the coupling of three phonons (four-phonon process).

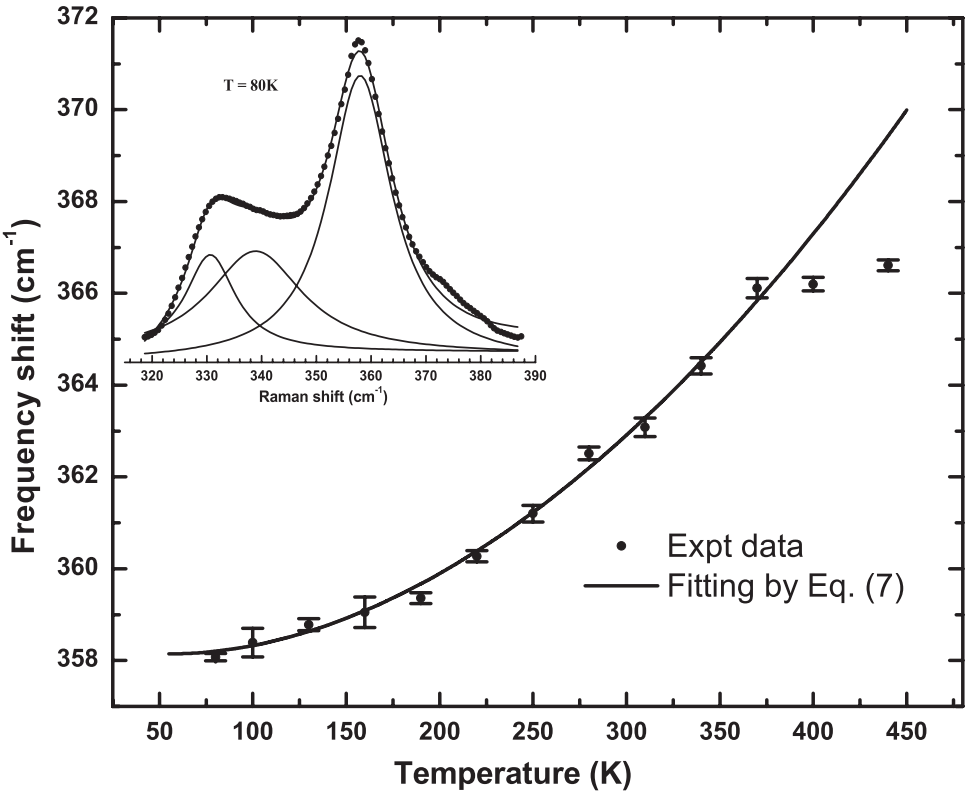

FIG. 8. Frequency shift of $T_g + A_g$ mode as a function of temperature. The solid line represents the calculated frequency shift using equation (7). Inset shows the fitting of $T_g + A_g$ mode at 80 K using DHO model (Equation (10)).

A and B are the fitting parameters. The multi-phonon processes associated with the cubic terms give rise to a negative frequency shift; whereas, the shift associated with quartic anharmonicity can be either positive or negative. The resultant frequency shift due to phonon-phonon interaction may be either positive or negative depending on the relative magnitudes of the anharmonic terms in the inter-atomic potential.

In our experimental observation, the resultant shift towards higher frequency side; i.e. the positive quatric anharmonicity dominates over the volume expansion effect and third order anharmonicity in the studied temperature range of 80–440 K. The Raman profile of $T_g + A_g$ mode obtained at different temperatures was fitted by using damped harmonic oscillator (DHO) model as.[33]

$$I(\omega) = \left[\chi_0 \Gamma_0 \omega \omega_0^2 (\bar{n} + 1)\right] / \left[\left(\omega_0^2 - \omega^2\right)^2 + \omega^2 \Gamma^2\right] \quad (10)$$

Where, ω_0 is the peak frequency, Γ_0 is the line width, χ_0 is related to the peak intensity, and $n = exp(-\hbar\omega/k_B T) - 1$, is the Bose-Einstein factor of phonon frequency ω. It is well known that the bands related to first order Raman scattering should have different temperature dependencies. For the first order Stokes process, the intensity is directly proportional to $(\bar{n} + 1)$, hence, simple Lorentz function is not suitable for the fitting of Raman profile as a function of temperature.

As mentioned, the temperature dependent frequency shift of $T_g + A_g$ in Fig. 8 shows strong frequency hardening with increasing temperature up to ~350 K, i.e. below the Debye temperature (T_D) 385K of Yb_2O_3. Above the Debye temperature, the hardening process slows down. We have fitted the experimental data points (solid circles) by using equation (7) and the solid line depicts the fitted curve. The error bars represent the standard error of measuring the experimental frequency at different temperatures. The temperature dependent parameters so obtained, are listed in the Table II. At lower temperatures ($T < T_D$) the main contribution to the hardening is due to the positive quatric anharmonicity. We have calculated the total anharmonicity (listed in Table II) of $T_g + A_g$ mode using

TABLE II. Best-fit values for anharmonic constants, true and quasi-harmonic contribution in $T_g + A_g$ mode of Yb_2O_3.

Raman Mode	ω_0 (cm^{-1})	A (cm^{-1})	B (cm^{-1})	$\frac{d\omega}{dT}$ ($cm^{-1}K^{-1}$)	$\left(\frac{1}{\omega_i}\frac{d\omega_i}{dT}\right)_P$ (K^{-1})	$\left(\frac{1}{\omega_i}\frac{d\omega_i}{dT}\right)_V$ (K^{-1})	$\gamma_i\alpha$ (K^{-1})
$T_g + A_g$	356.8	−0.21	0.63	0.033	8.17×10^{-5}	9.19×10^{-5}	1.02×10^{-5}

the formula[34]

$$\left(\frac{1}{\omega_i}\frac{d\omega_i}{dT}\right)_P = \left(\frac{1}{\omega_i}\frac{d\omega_i}{dT}\right)_V - \gamma_i\alpha \tag{11}$$

The first term on the right hand side describes the true anharmonic contribution and second, quasi-harmonic term. Above the Debye temperature, the hardening process slows down due to the increasing opposite effect of quasi-harmonicity arising from the thermal expansion and cubic anharmonicity.

IV. CONCLUSIONS

We have investigated the response of the optical phonons of cubic Yb_2O_3 powder as a function of pressure and temperature. The cubic Yb_2O_3 transforms to the hexagonal phase at and above 20.6 GPa. However, the mixed phase of cubic and hexagonal was identified at and above ∼11 GPa. The phase transition is irreversible as observed after release of pressure. We have identified the sharp intra-band electronic transition between the split unfilled f-orbital of Yb^{3+} ions sitting at C_{3i} sites. The temperature dependencies of the optical modes of Yb_2O_3 show an unusual hardening with increasing temperature. Using the mode Gruneisen parameter calculated from the high pressure data, we have calculated the true anharmonicity and quasi-harmonicity of the most dominating $T_g + A_g$ mode of Yb_2O_3; the temperature dependent data analysis reveals that this mode is truly anharmonic, i.e. $(\Delta\omega)_{anh}$ is the dominant factor, and leads to the unusual/anomalous mode hardening observed in the present case and this phenomenon arises from dominating quatric phonon-phonon interaction.

ACKNOWLEDGMENTS

The authors are grateful to CSIR for research grant (network project NWP-45) and Director, National Physical Laboratory for encouragement. We are thankful to Dr. S. M. Sharma and Mr. H. Poswal in BARC, Mumbai for facilitating high pressure Raman measurements.

[1] M. Mikami and S. Nakamura, J. Alloys Compd. **208**, 687 (2006).
[2] A. Ubaldini and M. M. Carnasciali, J. Alloys Compd. **454**, 374 (2008).
[3] E. Antic-Fidancev, J. Hölsa, and M. Lastusaari, J. Alloys Compd. **341**, 82 (2002).
[4] T. Jüstel, J. C. Krupa, and D. U. Wiechert, J. Lumin. **93**, 179 (2001).
[5] F. Uchinakawa and J. D. Mackenzi, J. Mater. Res. **4**, 787 (1989).
[6] G. Schaack and J. A. Koningstein, J. Opt. Soc. Am. **60**, 1110 (1970).
[7] C. Meyer, J. P. Sanchez, J. Thomasson, and J. P. Itié, Phys. Rev. B **51**, 12187 (1995).
[8] Q. X. Guo, Y. S. Zhao, C. Jiang, W. L. Mao, Z. W. Wang, J. Z. Zhang, and Y. J. Wang, Inorg. Chem. **46**, 6164 (2007).
[9] D. Liu, W. Lei, Y. Li, Y. Ma, J. Hao, X. Chen, Y. Jin, D. D. Liu, S. Yu, Q. L. Cui, and G. T. Zou, Inorg. Chem. **48**, 8251 (2009).
[10] D. Lonappan, N. V. Chandra Shekar, T. R. Ravindran, and P. C. Sahu, Mater. Chem. Phys. **120**, 65 (2010).
[11] E. Husson, C. Proust, P. Gillet, and J. P. Itié, Mater. Res. Bull. **34**, 2085 (1999).
[12] H. R. Hoekstra and K. Gingerich, Science **146**, 1163 (1964).
[13] H. R. Hoekstra, Inorg. Chem. **5**, 754 (1966).
[14] T. Atou, K. Kusaba, K. Fukuoka, M. Kikuchi, and Y. Syono, J Solid State Chem. **89**, 378 (1990).
[15] Q. Guo, Y. Zhao, C. Jiang, W. L. Mao, Z. Wang, J. Zhang, and Y. Wang, Inorg. Chem. **46**, 6164 (2007).
[16] T. Hongo, K. Kondo, K. G. Nakamura, T. Atou, J Mat. Sci. **42**, 2582 (2007).
[17] H. Chen, C. He, C. Gao, Y. Ma, J. Zhang, X. Wang, S. Gao, D. Li, S. Kan, and G. Zau, J Phys.:Condens. Matter **19**, 425229 (2007).
[18] M. W. Urban and B. C. Cornilsen, J. Phys. Chem. Solids **48**, 475 (1987).
[19] N. Dilawar, D. Varandani, V. P. Pandey, M. Kumar, S. M. Shivaprasad, P. K. Sharma, and A. K. Bandyopadhyay, J. Nanosci. Nanotechnol. **6**, 105 (2006).

[20] N. Dilawar, D. Varandani, S. Mehrotra, H. Poswal, S. M. Sharma, and A. K. Bandyopadhyay, Nanotechnology, **19**, 115703 (2008).
[21] N. D. Sharma, J. Singh, S. Dogra, D. Varandani, H. K. Poswal, S. M. Sharma, and A. K. Bandyopadhyay, J. Raman Spectrosc. **42**, 438 (2011).
[22] H. Yusa, T. Kikegawa, and T. Tsuchiya, Photon Factory Report, **27** PartB 195 (2010).
[23] D. Lonappan, http://ir.inflibnet.ac.in:8080/jspui/bitstream/10603/9923/10/10_chapter 5.pdf, Ph.D Thesis, IGCAR, India (2012).
[24] W. B. White and V. G. Keramidas, Spectrochimica Acta **28A**, 501 (1972).
[25] J. B. Gruber, R. D. Chirico, and E. F. Westrum, Jr., J. Chem. Phys. **76**, 4600 (1982).
[26] H. J. Schugar, E. I. Solomon, W. L. Cleveland, and L. Goodman, J. Am. Chem. Soc. **79**, 6442 (1975).
[27] J. Gouteron, D. Michel, A. M. Lejus, and J. Zarembowitch, J. Sol. Stat Chem. **38**, 288 (1981).
[28] S. Jiang, J. Liu, C. Lin, L. Bai, W. Xiao, Y. Zhang, D. Zhang, X. Li, Y. Li, and L. Tang, J. Appl. Phys. **108**, 083541 (2010).
[29] F. X. Zhang, M. Lang, J. W. Wang, U. Becker, and R. C. Ewing, Phys. Rev. B. **78**, 064114 (2008).
[30] S. M. Sharma and S. K. Sikka, Prog. Mater. Sci. **40**, 1 (1996)
[31] H. Tang and I. P. Herman, Phys. Rev. B **43**, 2299 (1991).
[32] M. Balkanski, R. F. Wallis, and E. Haro, Phys. Rev. B **28**, 1928 (1983).
[33] K. Samanta, P. Bhattacharya, and R. S. Katiyar, Phys. Rev. B **75**, 035208 (2007).
[34] K. Kamali, T. R. Ravindran, C. Ravi, Y. Sorb, N. Subramanian, and A. K. Arora, Phys. Rev. B **86**, 144301 (2012).